



# CHORUS

This is the accepted manuscript made available via CHORUS. The article has been published as:

## Exploring Low Internal Reorganization Energies for Silicene Nanoclusters

Ricardo Pablo-Pedro, Hector Lopez-Rios, Jose-L. Mendoza-Cortes, Jing Kong, Serguei Fomine, Troy Van Voorhis, and Mildred S. Dresselhaus

Phys. Rev. Applied **9**, 054012 — Published 9 May 2018

DOI: [10.1103/PhysRevApplied.9.054012](https://doi.org/10.1103/PhysRevApplied.9.054012)

# Exploring Low Internal Reorganization Energies for Silicene Nanoclusters

*Ricardo Pablo-Pedro<sup>1</sup>, Hector Lopez-Rios<sup>2</sup>, Jose-L Mendoza-Cortes<sup>3,4</sup>, Jing Kong<sup>5</sup>, Serguei  
Fomine<sup>6</sup>, Troy Van Voorhis<sup>7</sup>, and Mildred S. Dresselhaus<sup>5,8</sup>*

<sup>1</sup>Department of Chemistry, Massachusetts Institute of Technology, 77 Massachusetts Avenue, Cambridge, MA 02139, United States

<sup>2</sup>Instituto de Investigaciones en Materiales, Universidad Nacional Autónoma de México, Apartado Postal 70-360, CU, Coyoacán, Ciudad de México 04510, México

<sup>3</sup>Department of Chemical & Biomedical Engineering, Florida A&M University and Florida State University, Joint College of Engineering, Tallahassee FL, 32310, USA

<sup>4</sup>Department of Physics & Scientific Computing Department, Materials Science and Engineering Program, High Performance Material Institute, Condensed Matter Theory, National High Magnetic Field Laboratory, Florida State University, Tallahassee FL, 32310, USA

<sup>5</sup>Department of Electrical Engineering and Computer Science, Massachusetts Institute of Technology, Cambridge, MA 02139, United States

<sup>6</sup>Department of Physics and Department of Electrical Engineering and Computer Science, Massachusetts Institute of Technology, Cambridge, MA 02139, United States

## Abstract

High-performance materials rely on small reorganization energies to facilitate both charge separation and charge transport. Here, we performed DFT calculations to predict small reorganization energies of rectangular silicene nanoclusters with hydrogen-passivated edges denoted by H-SiNC. We observe that across all geometries, H-SiNCs feature large electron affinities and highly stabilized anionic states, indicating their potential as n-type materials. Our findings suggest that fine-tuning the size of H-SiNCs along the “zigzag” and “armchair”

directions may permit the design of novel n-type electronic materials and spintronics devices that incorporate both high electron affinities and very low internal reorganization energies.

## Introduction

Graphene has attracted increasing interest since its discovery for its potential as a future elementary unit in modern microelectronics, such as field-effect transistors<sup>1</sup>, photovoltaic cells<sup>2</sup>, advanced gas sensors<sup>3</sup>, and battery energy storage<sup>4</sup>. Additionally, the isolation of graphene has inspired the new world of two-dimensional (2D) materials, where some recent members include black phosphorus<sup>5</sup>, transition metal dichalcogenides (TMDs)<sup>6</sup>, and silicene<sup>7</sup>. Among these 2D materials, silicene has been predicted to possess most of the remarkable electronic properties of graphene, such as Dirac cone, carrier mobility, and high Fermi velocity<sup>7</sup>. Moreover, the major advantage of investigating silicene is that it can be easily incorporated into the present silicon-based microelectronics industry<sup>8,9</sup>. In this direction, considerable improvements have been achieved in the use of silicene as field-effect transistors at room temperature<sup>10</sup> and in spintronics applications<sup>11</sup>.

Interestingly, the electronic properties of silicene change in a nontrivial manner when going to lower dimensions. Silicene nanoribbons, for instance, can be either metals or semiconductors depending on width<sup>9</sup>. For the case of silicene nanoclusters, the electronic structure is expected to be different from pristine silicene and nanoribbons because there are additional degrees of freedom from the edge atoms<sup>8</sup>. In addition, silicene nanoclusters have the advantage that they all possess fine band gaps because of quantum confinement effect that is desirable for their applications. The fabrication of these silicene nanostructures could be realized using etching techniques that have been already used in cutting graphene sheets into nanostructures with desired shape and size. This experimental progress motivates our study of electronic structure of silicene nanoclusters with rectangular shape<sup>12,13</sup>.

Carrier transport is the central property for applications of silicene in field-effect transistors,

thermoelectric devices, and spintronics. Therefore, having high carrier mobility is very important for developing new silicene nanoelectronic devices. The transport mechanism is generally understood with respect to the limiting cases of hopping (polaron) transport and band-like transport corresponding to the extreme localization or delocalization of the charge carriers. The band-like regime is generally observed only at low temperatures in highly ordered samples (i.e. the mobility  $\mu$  decreases with temperature as  $\mu \propto T^{-n}$ ) up to room temperature<sup>14</sup>. **The** hopping (polaron) mechanism **consists with** the carrier is localized on one molecule through the formation of a self-trapped state (a polaron) and transport occurs through a thermally activated hopping mechanism ([strong electron-phonon coupling](#)), which is observed commonly in small molecules and molecular semiconductors at high temperatures<sup>15</sup>. [For instance, the electron-phonon interaction of silicene is considerable, as the larger Si-Si interatomic distance of silicene, compared to graphene, weakens the pi-pi overlaps and results in a low-buckled structure with sp3-like hybridation<sup>7</sup>.](#) Then, because of the size of our [silicene](#) nanocluster and [large geometry geometry relaxations of the silicene nanoclusters](#), we consider that they could be described by the hopping [mechanism in which](#) the mobility ( $\mu$ ) of the charge carriers (electrons or holes) is directly proportional to the transfer rate ( $k$ ) of charge carriers described by the [Einstein](#) relation<sup>16</sup>

$$\mu = \frac{eA^2}{k_B T} k \quad (1)$$

Where  $k_B$ , T, e and A are the Boltzmann constant, temperature, the electron charge, and the hopping transport distance. According to the Marcus-Huss semiclassical model for the inter-chain charge transfer, the charge transfer rate is given by<sup>16</sup>

$$k = \frac{2\pi}{h} \left( \frac{\pi}{\lambda k_B T} \right)^{-1/2} H_{ab}^2 e^{-\left( \frac{\lambda}{4k_B T} \right)^2} \quad (2)$$

Here  $h$ ,  $\lambda$ , and  $H_{ab}$  are the Plank constant, the reorganization energy and the electronic coupling matrix element between the donor and acceptor, respectively. According to Eq. 2, the charge transfer is determined by  $H_{ab}$  and  $\lambda$ . However,  $H_{ab}$  starts to saturate for oligomers with more than 5 monomeric units indicating the exponential contribution in Eq. 2 keep increasing and for more than 7 monomeric units it dominates the behavior of the charge transfer rate<sup>17</sup>. Therefore, the key parameter that governs the behavior of the charge transfer rate is the reorganization energy which decreases with increasing length of the system, as will be discussed below. At some point the transfer coupling is expected to saturate once it depends on the conjugation length of polymers<sup>16</sup>. Then, for large conjugated polymers and organic molecular semiconductors, the exponential nature of Eq. 2 dominates and in this way, the reorganization energy is the most important parameter to be studied to estimate the charge carrier transport. The reorganization energy,  $\lambda$ , corresponds to the energy of structural change when going from neutral-state geometry to charged-state geometry and vice versa. In terms of the electron-phonon mechanism,  $\lambda$  is a measure of the strength of the electron-phonon interaction and produces a relation between the geometry, the electronic structure, and the transport properties of the material<sup>18</sup>. The reorganization energy can be divided in terms of the transport of holes ( $\lambda_h$ ) and electrons ( $\lambda_e$ ) in order to determine whether a material may have a greater mobility of electrons than holes or of holes than electrons, respectively. It is known that most organic semiconductors have hole reorganization ( $\lambda_h$ ) energies greater than 0.1 eV, however several hole-transporting (*p*-type) organic semiconductors have been reported with hole reorganization energies of less than 0.1 eV, for example, pentacene (0.097 eV)<sup>19</sup> and circum(oligo)acenes (0.057 to 0.127 eV)<sup>20</sup>. On the other hand, studies of electron-transporting (*n*-type) semiconductors have been limited in the last decade because of the instability in air of radical anionic semiconductors and the high injection barrier of electrons. One of the few examples include fullerene (C<sub>60</sub>), which has been found to be an excellent *n*-type acceptor with a small electron reorganization energy of  $\lambda_e = 0.060$  eV<sup>21</sup>. This allows fast photoinduced charge separation and slow charge recombination resulting in the

formation of a long-lived charge-separated state with high quantum yield<sup>22</sup>. The small reorganization energy of fullerene can also be ascribed to its extended  $\pi$ -conjugation and its rigid molecular structure. In general, the hole ( $\lambda_h$ ) and electron ( $\lambda_e$ ) reorganization energy decreases as the size of the  $\pi$  conjugated system is increased. For instance, anthracene  $\lambda_h = 0.137$  eV and  $\lambda_e = 0.196$  eV; tetracene, 0.113 eV and 0.160 eV; and pentacene, 0.097 eV and 0.132 eV,<sup>23</sup> respectively.

In anisotropic two-dimensional (2D) semiconductors such as TMDs<sup>24,25</sup>, black phosphorus<sup>26,27</sup>, and silicene<sup>8</sup>; the electrons and phonons behave differently in different in-plane directions, e.g., armchair and zigzag directions. This leads to angle-dependent mechanical, optical, and electrical responses. Therefore, we hypothesized that the reorganization energies in anisotropic materials should exhibit different behaviors along different directions. These unique properties may permit the design of novel electronics and optoelectronics with anisotropic crystalline orientation.

In this work, we study reorganization energies of H-SiNCs along different directions by using density functional theory (DFT). The values of the reorganization energies for H-SiNCs are obtained by varying the width of the zigzag and the armchair directions. To further evaluate these H-SiNCs, we computed the adiabatic electron affinities (EAs) and the ionization potential (IP) energies. To the best of our knowledge, this is the first theoretical work exploring the reorganization energies for different directions of rectangular silicene nanoclusters.

## Computational Details

We have carried out geometrical optimizations of rectangular silicene nanoclusters utilizing the three-parameter Becke and Lee-Yang-Parr functional (B3LYP) in conjunction with Dunning's correlation-consistent cc-pVDZ basis set for all atoms. For all molecules we used restricted DFT (RB3LYP) or unrestricted DFT (UB3LYP) when specified. Grimme's D3 dispersion correction<sup>28</sup>

was also used in all DFT calculations to account for the dispersion interactions. Thus, the methods are named RB3LYP-D3 and UB3LYP-D3; we indicate in the text if only one method is used. The need for UB3LYP-D3 is due to the singlet-triplet instability detected in the model's optimized closed-shell singlet state wave function, also necessitating the consideration of two different values of multiplicities, singlet and triplet states. Here, a singlet state is an electronic state such that all electron spins are paired (anti-ferromagnetic state) while in a triplet state the electron that is promoted has the same spin orientation (parallel) to the other unpaired electron (ferromagnetic state). Singlet and triplet spin values are derived using the equation for multiplicity,  $2S+1$ , where S is the total spin angular momentum (sum of all electron spins in the molecule). The closed-shell singlet systems that presented triplet instability were re-optimized using a broken-symmetry unrestricted (UBS) method<sup>29</sup>. Additionally, frequency calculations for selected H-SiNCs were performed to ensure the absence of any vibrational instabilities in the ground state structures. None of the systems analyzed have negative frequencies, which means that they are thermodynamically stable. The calculations were performed using the code TURBOMOLE V7.0<sup>30</sup>. From here on, we will denote UB3LYP-D3 method as B3LYP for simplicity.

We also ran complete active-space self-consistent field (CASSCF) calculations of the charged molecules of the corresponding electronic multiplicity also using the B3LYP functional to explore their multi-configurational character. This is due to correct and compare, if needed, for the multi-configurational character of the neutral H-SiNCs reported in a previous study<sup>8</sup> at the B3LYP level of theory. In addition, we ran CASSCF calculations in order to revise the correlation between the UB3LYP and CAS level of theory<sup>31</sup>. They both showed that anionic species are the most stable species compared with the cationic species as shown in the supporting information. Hence, the computations for the silicene nanoclusters at complete active space self-consistent field level support the conclusions obtained at the DFT level. The chosen active spaces consisted of 9 electrons and 10 orbitals, and 11 electrons and 10 orbitals, for cation and anion radicals, respectively. The selection of the active space was simple, since all pi orbitals

form the correct active space, the more orbitals one includes the better is its description. We included as many orbitals as possible from the computational point of view. Since, most of the systems have only two or three most important configurations, we used an active space consisting of more than 100000 configurations that seems to be adequate from our point of view. In addition, we visualized the corresponding orbitals to ensure that they involve all atoms of studied systems, and we inspected the density matrix generated in each calculation to ensure that all active orbitals have population numbers between 0.1 and 1.9, a confirmation of [a](#) correctly selected active space. The 6-31G(d) basis set was assigned to all atoms. These calculations were carried out with Gaussian 09 rD.01. code<sup>32</sup>.

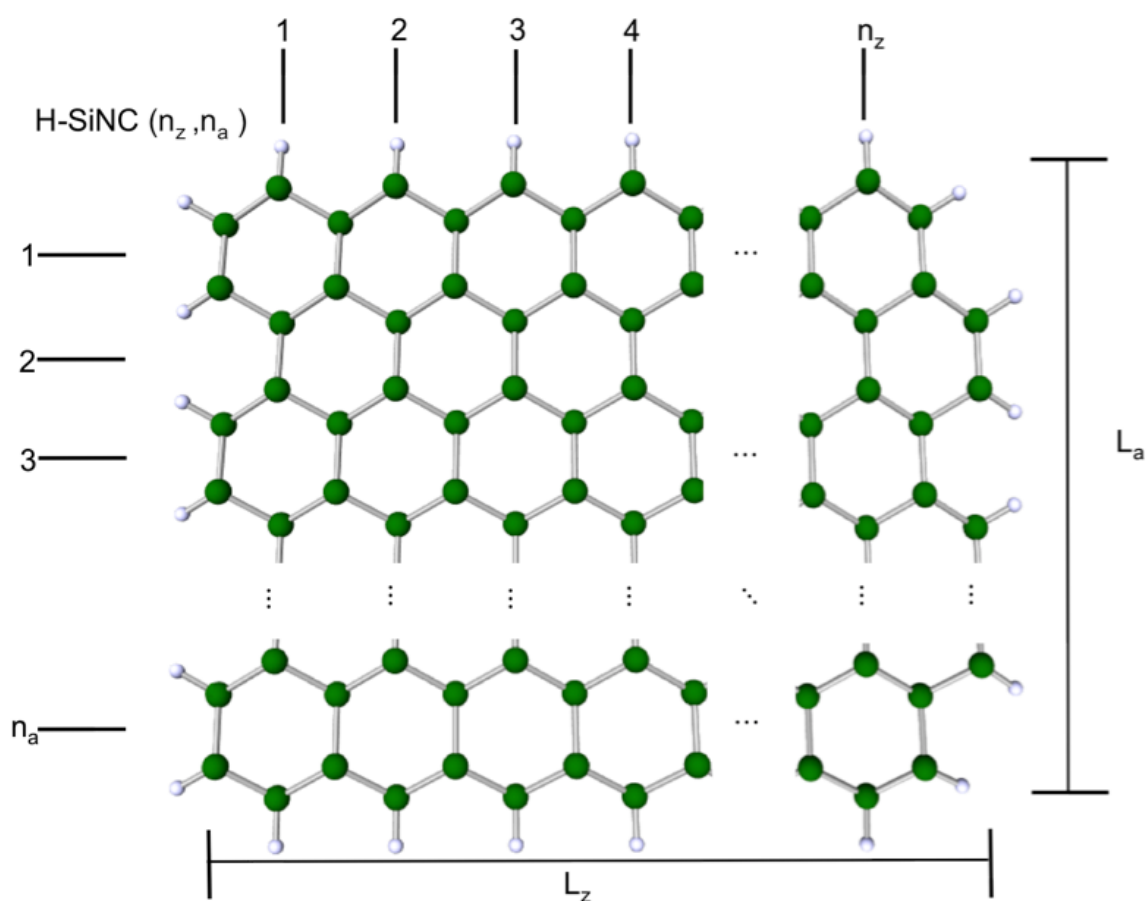


**Figure 1.** Top-down view of a lattice structure of silicene, where the edges are passivated with hydrogen. The  $n_x$  and  $n_y$  are the number of fused benzene rings in columns and rows.

We study rectangular silicene nanoclusters following the pattern shown in Figure 1. All edge dangling bonds were passivated with hydrogen. To specify the size of each H-SiNC, we use  $n_x$  and  $n_y$ , which correspond to the number of hexagonal units along the zigzag and armchair edges.

Here we define a [characteristic area scale](#) by  $N = n_x \times n_y$ , which corresponds to the total of fused rings in the silicene nanocluster. The characteristic dimensions of each H-SiNC are denoted here by  $L_x$  (armchair edge) and  $L_y$  (zigzag edge), being linear functions of  $n_x$  and  $n_y$ , and the average Si-Si bond length. We vary  $n_x$  from 1 to 9 (which means that  $L_x$  varies from 0.439 nm for  $n_x=1$  to 3.112 nm for  $N=9$ , approximately) and for  $n_y$  from 1 to 7 ( $L_y$  varying from 0.381 nm for  $n_y=1$  to 2.882 nm for  $n_y=7$ ).

The geometry of every silicene nanocluster was first optimized for the neutral molecule at the B3LYP level,  $E_0(q_0)$ . The energy was then calculated for the negatively charged molecule (adding an electron to the neutral molecule) in the optimized geometry of the neutral molecule,  $E_-(q_0)$ . The geometry of the negatively charged molecule was subsequently optimized to obtain  $E_-(q_-)$ . Their energy difference,  $E_-(q_0) - E_-(q_-)$ , is equal to the reorganization energy  $\lambda_-$ , see Fig. 2. We now remove an electron from the optimized negatively charged molecule, and calculate the energy without relaxing the geometry to obtain the  $E_0(q_-)$  state. The energy difference between the  $E_0(q_-)$  state and the optimized neutral molecule  $E_0(q_0)$  is the reorganization energy  $\lambda_+$ , as shown in Fig. 2. Then, the total electron reorganization energy for the process is equal to<sup>33</sup>

$$\lambda_- = \lambda_2 + \lambda_1 = [E_0(q_-) - E_0(q_0)] + [E_-(q_0) - E_-(q_-)] \quad (3)$$

where  $E$  is energy and  $q$  is the geometry. The subscripts 0 and  $-$  represent the neutral and anionic states, respectively. The same procedure was carried out for the cation state. Thus, the hole

reorganization energy is given by<sup>33</sup>

$$\lambda_+ = \lambda_4 + \lambda_3 = [E_0(q_+) - E_0(q_0)] + [E_+(q_0) - E_+(q_+)] \quad (4)$$

Here  $E$  is energy and  $q$  is the geometry as in Eq. 3. The subscripts 0 and + represent the neutral and cationic states, respectively. Moreover, we used total-energy differences between the DFT-B3LYP calculations performed for the neutral and charged systems to evaluate: (i) the adiabatic ionization potentials (IPs) and electron affinities (EAs); (ii) the highest occupied molecular orbital (HOMO) and lowest unoccupied molecular orbital (LUMO) energies for the neutral systems. The vertical transitions involved in Equations 3 and 4 are shown in Figure 2.

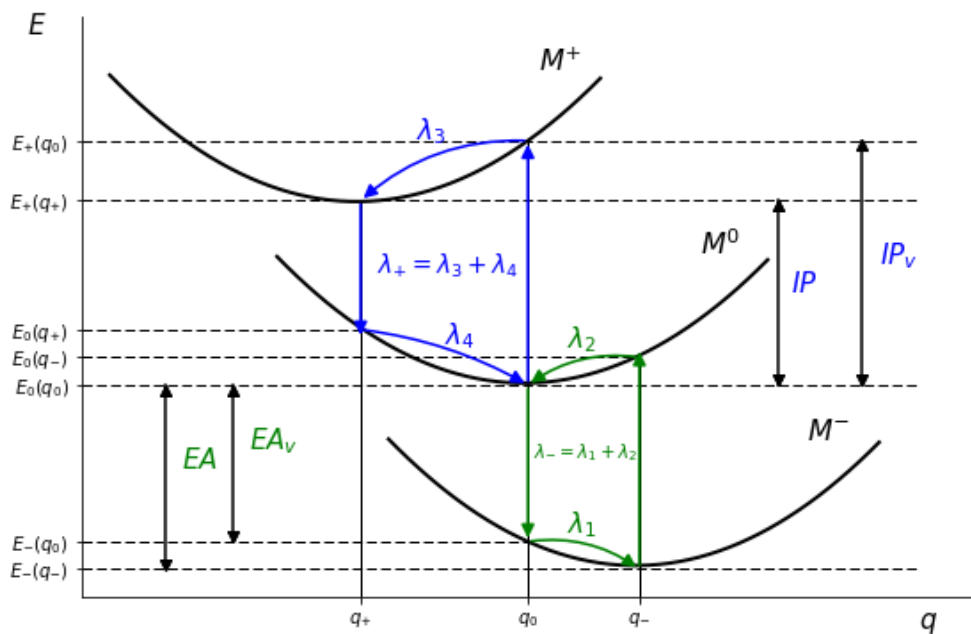


**Figure 2.** Potential energy surfaces sketch for the neutral ( $M^0$ ), negatively ( $M^-$ ) and positively ( $M^+$ ) charged structures.  $E$  is the energy,  $q$  is the geometry, and the subscripts 0, -, and + denote neutral, anionic and cationic states, respectively. Here IP is the ionization potential, EA is the electron affinity, and the subscript  $v$  denotes vertical energy transitions.

# Results and discussion

We summarize the optimized bond lengths of ground, cationic, and anionic states for selected H-SiNC( $n_z, n_a$ ) in Table 1 at the B3LYP/cc-pVDZ level of theory. Two multiplicities were used according to previous results, i.e., single (S=0) and triplet (S=1). The bond length increases (decreases) in going from the neutral to the negatively (positively) charged structure show a consistent trend along the series. Overall, small molecules show the largest geometry relaxations, e.g., H-SiNC(2,1) changes its Si-Si bond lengths approximately 0.025 Å. This value is reduced to 0.005 Å and 0.002 Å in H-SiNC(7,1) and H-SiNC(5,4), respectively. However, the geometry distortions in the buckled structure of the silicene nanoclusters are larger than in the Si-Si bond lengths with averaged differences in the range of  $\pm 0.03$  Å, indicating that even for a large system, e.g., H-SiNC(5,4), the neutral molecule will suffer large height modifications in its charged species, as shown in Fig. 3. Compared to the neutral geometry, the cationic geometry shrinks via the shortening of both bonds and heights, and the anionic geometry expands via lengthening of the bonds and heights. These geometry distortions (i.e. bond lengths and heights) of the H-SiNCs could explain why in some silicene nanoclusters the small reorganization energies are small (see the supplementary information). In terms of  $\pi$ -conjugation, larger silicene nanoclusters possess an extensive  $\pi$  conjugation that leads to greater delocalized charge distribution. Thus, local structural adjustment (i.e., bond length and height) for electron transfer ( $\lambda$ ) is less severe in large silicene systems than smaller systems; see the Si-Si bond lengths and heights ( $\Delta_a$ ) in Table 1. In general, for the H-SiNCs, the largest structural changes are observed in the average height of the anions.

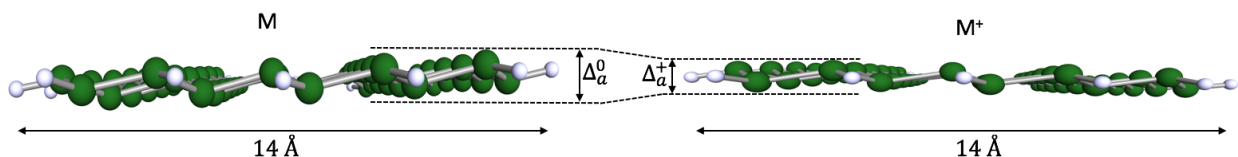


**Figure 3.** Neutral state (left) of H-SiNC(5,4) relaxes into a new structure (right) when one electron is removed. As a result, the silicene nanocluster contracts along the vertical axis. The displacement is magnified 2 times in order to make this distortion clear.

We summarize the calculated hole ( $\lambda_h$ ) and electron ( $\lambda_e$ ) reorganization energies, the adiabatic values of electron affinity (EA), and the ionization potential (IP) for the rectangular silicene nanoclusters in Table 2 at the B3LYP level of study. It has been demonstrated that the B3LYP functional used for the reorganization energy calculations best reproduces the experimental data for conjugated organic systems<sup>34,35</sup>. In addition, the B3LYP functional was found to reproduce reliable EAs for 14 atoms and 96 molecules<sup>36</sup>.

**Table 1.** The average Si-Si bond lengths ( $d_a$ ) and the average height ( $\Delta_a$ ) of selected neutral, cationic and anionic silicene structures at the B3LYP level of calculation. Here the subscripts 0, +, and - represent the neutral, cationic, and anionic states, respectively. Here S represents the initial triplet and singlet states.

H-SiNC( $n_z, n_a$ )	S	$d_a^0[A]$	$d_a^+[A]$	$d_a^-[A]$	$\Delta_a^0[A]$	$\Delta_a^+[A]$	$\Delta_a^-[A]$
(2,1)	0	2.254	2.251	2.279	0.459	0.396	0.572
(7,1)	0	2.264	2.260	2.269	0.441	0.420	0.479
(5,4)	0	2.271	2.269	2.273	0.480	0.467	0.489
(4,7)	0	2.272	2.270	2.273	0.482	0.473	0.487
(4,9)	0	2.272	2.271	2.273	0.480	0.475	0.484
(4,9)	1	2.272	2.271	2.273	0.480	0.474	0.488

The adiabatic IPs and EAs presented in Table 2 were computed from the difference in the total energy between the optimized neutral state and the corresponding optimized cation or anion state, i.e.,  $IP = E_c(q_c) - E_0(q_0)$  and  $EA = E_0(q_0) - E_a(q_a)$ <sup>37</sup>. For all the studied H-SiNCs, the cationic-state potential energy was higher than the neutral-state potential energy giving a positive IP. Moreover, it is observed that the IPs of the H-SiNCs drop with the number of fused rings, N,

which is in agreement with other conjugated systems. In the case of the EAs, all H-SiNCS will bind an electron with a positive EA, which also increases along with the number of benzoic rings. For *n*-type organic semiconductors, the adiabatic EA is an important property that determines organic field-effect transistor device performance such as durability. Among the studied systems, a few H-SiNCs exhibit quite large adiabatic EAs, exceeding the threshold of 2.80 eV used for classifying *n*-type materials<sup>38,39</sup>. Hence, H-SiNCs are expected to be stable electron transport materials<sup>40</sup>.

**Table 2.** Hole ( $\lambda_+$ ) and electron ( $\lambda_-$ ) reorganization energies, along with their adiabatic ionization potentials (IPs) and electron affinities (EAs) calculated at the B3LYP level of theory. Here  $S_{\text{initial}}$  represents the initial triplet and singlet states.

H-SiNC( $n_z, n_a$ )	N	$S_{\text{initial}}$	$\lambda_-$ [eV]	EAs[eV]	$\lambda_+$ [eV]	IPs[eV]
(1,1)	1	0	0.775	1.39	0.303	7.12
(2,1)	2	0	0.297	1.93	0.182	6.47
(3,1)	3	0	0.237	2.39	0.148	6.06
(4,1)	4	0	0.121	2.68	0.117	5.80
(5,1)	5	0	0.088	2.85	0.099	5.66
(6,1)	6	0	0.078	2.94	0.094	5.59
(7,1)	7	0	0.077	2.99	0.093	5.56
(2,2)	4	0	0.315	2.38	0.144	6.06
(3,2)	6	0	0.233	2.73	0.117	5.75
(4,2)	8	0	0.136	2.95	0.101	5.56
(5,2)	10	0	0.114	3.05	0.100	5.48
(6,2)	12	0	0.134	3.10	0.105	5.46
(7,2)	14	0	0.159	3.13	0.099	5.47
(3,3)	9	0	0.142	2.91	0.085	5.57
(4,3)	12	0	0.091	3.09	0.077	5.42
(5,3)	15	0	0.143	3.15	0.086	5.40

(6,3)	18	0	0.190	3.19	0.133	5.40
(7,3)	21	0	0.205	3.21	0.090	5.38
(4,4)	16	0	0.081	3.19	0.072	5.33
(5,4)	20	0	0.220	3.22	0.083	5.34
(6,4)	24	0	0.188	3.24	0.138	5.34
(7,4)	28	0	0.150	3.28	0.075	5.29
(4,5)	20	0	0.067	3.26	0.063	5.27
(4,6)	24	0	0.287	3.31	0.065	5.22
(4,7)	28	0	0.076	3.35	0.070	5.18
(4,8)	32	0	0.214	3.39	0.066	5.15
(4,9)	36	0	0.181	3.41	0.206	5.12
(4,7)	28	1	0.069	3.09	0.065	5.14
(4,8)	32	1	0.062	3.16	0.059	5.12
(4,9)	36	1	0.088	3.19	0.052	5.10

---

As seen in Table 2, almost all of the H-SiNCs have a larger  $\lambda_e$  value than  $\lambda_h$ . Contextualizing our results, linear silicene nanoclusters could be considered as analogous molecules with oligoacenes. For instances, we compared some  $\lambda_e$  values of linear H-SiNCs with some common polycyclic aromatic hydrocarbons, i.e.,  $C_{10}H_8$  ( $N = 2$ ),  $C_{14}H_{10}$  ( $N = 3$ ),  $C_{18}H_{12}$  ( $N = 4$ ), and  $C_{22}H_{14}$  ( $N = 5$ ) at B3LYP/6-31G\*\* level of theory, which are 0.187, 0.137, 0.113, and 0.097 eV<sup>12</sup>, respectively. These values are comparable with the corresponding silicene systems H-SiNC(2,1), 0.182 eV; H-SiNC(3,1), 0.148 eV; H-SiNC(4,1), 0.117 eV; and H-SiNC(5,1), 0.099 eV at the B3LYP level of theory. For some H-SiNCs, their hole and electron reorganization energies are less than 0.1 eV such as H-SiNC(4,5) and H-SiNC(4,7). For systems with an initial triplet ground state, we can obtain even smaller hole and electron reorganization energies that can be compared

to fullerene (0.06 eV). These low values suggest that the mobility along the armchair direction is greater than in the zigzag direction for these systems, with  $n_a > n_z$ . In addition, we can observe that the values of  $\lambda_e$  and  $\lambda_h$  for systems with an initial triplet ground ( $S=1$ ) state are similar. This similarity in the electron and reorganization energies may suggest that these specific systems could act as ambipolars or  $n$ -acceptor materials merely considering the calculated electron and hole reorganization energies and adiabatic EA values. From these results it can be concluded that the initial ground state's spin state of the H-SiNCs has a profound effect on the reorganization energy as seen for H-SiNC(4, $n$ ), with  $n=7-9$ .

To examine the effect of the number of fused rings on the electron transfer,  $\lambda_e$  is plotted for different H-SiNCs in Fig. 4 (a). Since we are comparing different orientations (i.e. armchair and zigzag directions), there is not a perfect relationship between electron reorganization energy and the number of fused rings, but there is a trend: electron reorganization generally decreased with increased  $N$ . At  $N = 24$  we observed that for H-SiNC(6,4) and H-SiNC(4,6) structures, the change on the length in the armchair and zigzag direction significantly affects the electron and hole reorganization energies. The greatest decrease in  $\lambda_e$  and  $\lambda_h$  was obtained from molecules with initial triplet spin multiplicity. Thus, these low reorganization energies indicate an advantage for the H-SiNCs to transport electrons or holes when coupled to an external device that either donates or withdraws electrons such as a field effect transistor (FET)<sup>10</sup>. Another observation from Table 2 is that  $\lambda_e$  follows the trend that larger clusters (more extended  $\pi$  conjugation) have smaller  $\lambda_e$  values. In the inset graph of Fig. 4, we illustrate the relationship between electron affinity (EA) and  $\lambda_e$ . It is observed that small H-SiNCs have low electron affinity and high electron reorganization energy. On the contrary, large H-SiNCs have high electron affinity and low electron reorganization energy, two important factors for good  $n$ -type materials<sup>33</sup>. In the case of linear or nearly linear H-SiNCs, Fig. 4 (b) shows that the reorganization energy for all H-SiNCs decreases as  $N$  increases. This relation is comparable with the  $\lambda \sim N$  relation derived for linear oligomers<sup>41</sup>, where  $N$  is the number of heterocyclic rings.

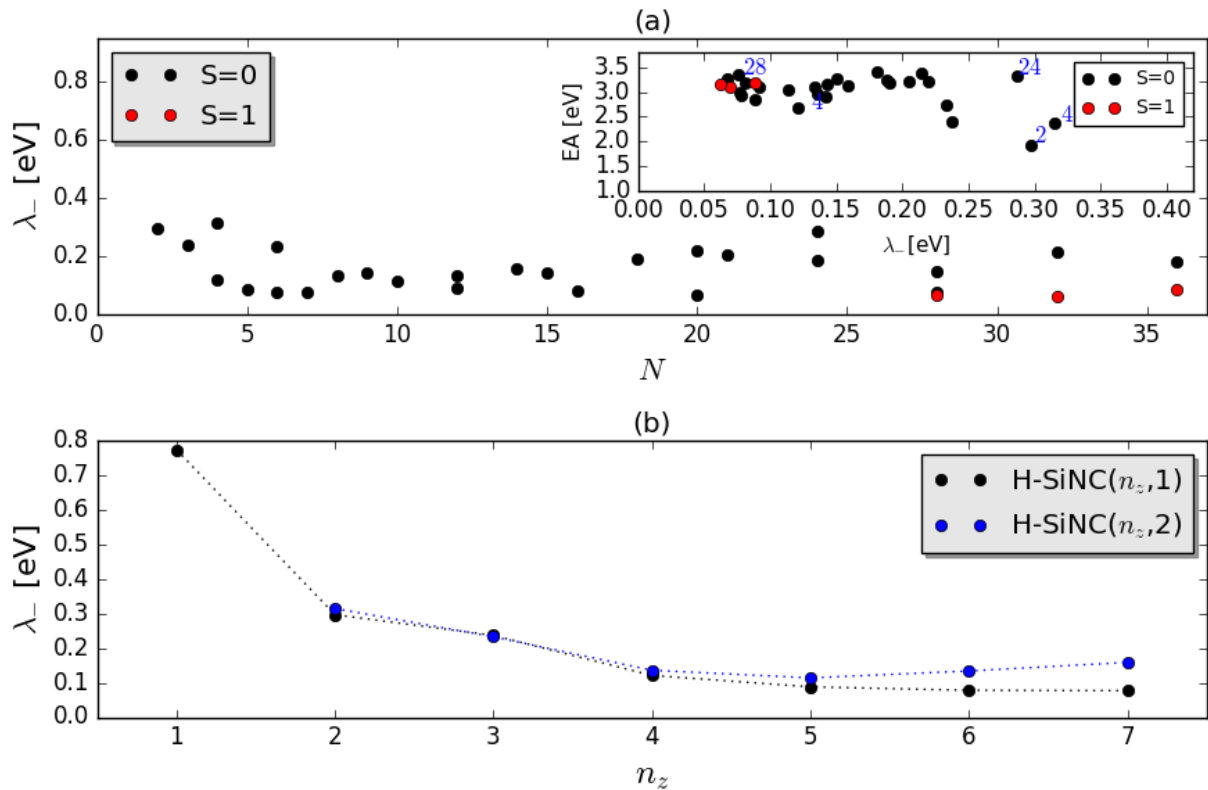


**Figure 4.** (a) Plot of electron reorganization versus number of fused rings  $N$  for H-SiNCs. Here  $S$  represents the initial spin for the triplet and singlet states for  $S = 1$  and  $S = 0$ , respectively. Inset: Plot of electron affinity (EA) versus electron reorganization energy ( $\lambda_-$ ). The numbers in the graph indicate the number of fused rings ( $N$ ) for selected H-SiNCs. (b) Plot of the electron reorganization energy versus number of fused rings along the zigzag direction for H-SiNCs with a singlet ground state.

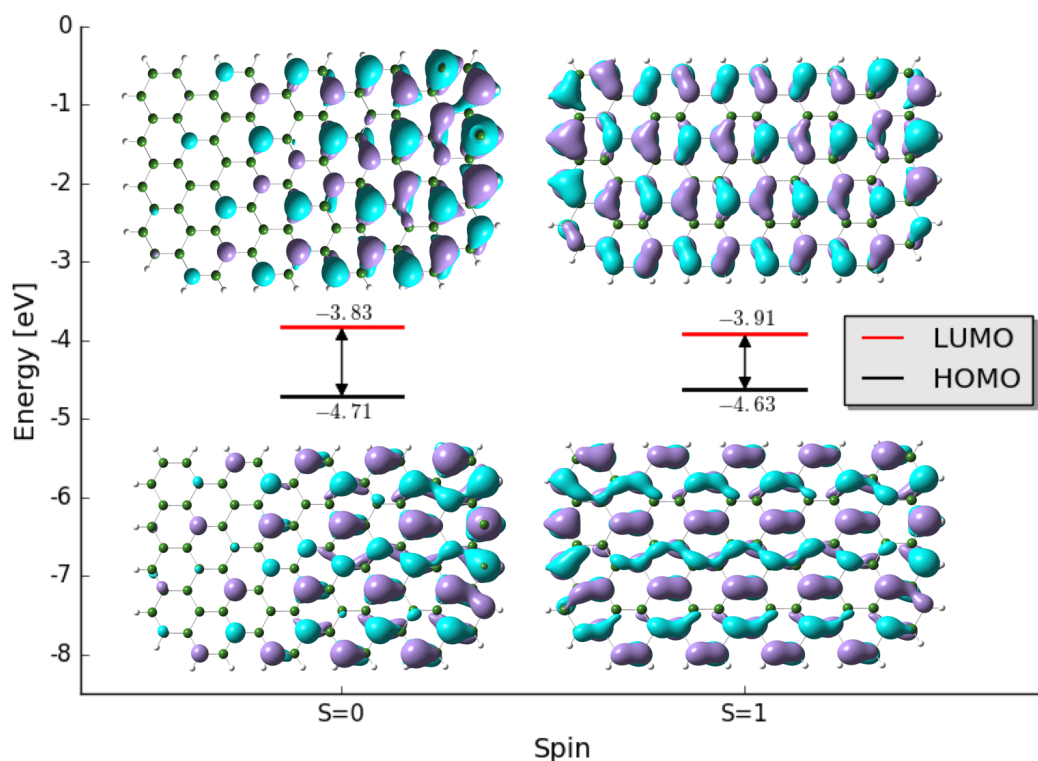


**Figure 5.** Frontier orbitals for neutral H-SiNC(4,9) with an initial singlet ( $S=0$ ), and triplet ( $S=1$ ) states at the B3LYP/cc-pVDZ level of theory. Molecular Orbitals were drawn with GaussView<sup>32</sup>.

From our results, we observed that critical geometric changes of the neutral molecule can occur when an electron is added to the LUMO ( $\lambda$ ) or when an electron it is removed from the HOMO ( $\lambda$ ). The extra electron or hole in the neutral molecule will induce localized charge defects in the form of polarons. The polaron binding energy is from the deformations in lattice and molecular geometries that occur as the carrier localizes on a given site. This quantity is thus closely linked to the reorganization energy in electron-transfer theories. This polaron energy arising from internal degrees of freedom can be obtained by expanding the site energy  $\epsilon_n$  in powers of molecular normal-mode coordinates, which can be calculated from the frontier molecular orbitals (HOMO and LUMO for hole and electron transport, respectively). In addition,

these geometric changes among charge transfer processes can correlate with the bonding character in the frontier orbitals<sup>33</sup>. This bonding character between two nearest atoms involving a molecular orbital is composed of bonding, antibonding, and nonbonding orbitals. For instance, adding an electron in the bonding orbital stabilizes the molecule because it is in between the atoms while adding an electron into the antibonding orbital will decrease the stability of the molecule. However, nonbonding only involves one atom, so the addition or removal of an electron does not change the energy or bond order (bond length alteration) of the molecule. Interestingly, it has been demonstrated that by having a high nonbonding character<sup>33</sup>, we can obtain low reorganization energies because nonbonding induces much less bond length adjustment than bonding and anti-bonding upon charge transfer. Therefore, to examine whether structural adjustments with charge transfer correlates with the spatial distribution of frontier orbitals of the H-SiNCs to obtain low reorganization energies; we show in Fig. 5 that the percentage of nonbonding character is smaller in the HOMO than in the LUMO for H-SiNC(4,9) with an initial singlet state (see the supplementary for more information about bond length alternations). Therefore, this factor should contribute to a larger value of  $\lambda_c$  than  $\lambda_a$ . Comparing the height of the cation and anion for H-SiNC(4,9) with  $S_{\text{initial}}=0$ , we observe that the height difference between the neutral and cation,  $|\Delta_{C-N}| = 0.005$  (Table 1), is larger than that of  $|\Delta_{A-N}| = 0.004$ , as with the values of  $\lambda_c$  relative to  $\lambda_a$ . In Figure 5, it is shown that when more extended delocalization is present for the initial triplet state molecule, the extended delocalization leads to the reduction of  $\lambda_c$  and  $\lambda_a$ . For H-SiNC(4,9) with  $S_{\text{initial}}=1$  ( see Fig. 5), it is noted that the values of  $|\Delta_{A-N}| = 0.008$  is larger than that of  $|\Delta_{C-N}| = 0.006$  ( Table 1), as with the values of  $\lambda_c$  relative to  $\lambda_a$ . Therefore, this shows how specific structural modifications such as bond length alterations are originated upon the removal and addition of an electron to the silicene nanoclusters.

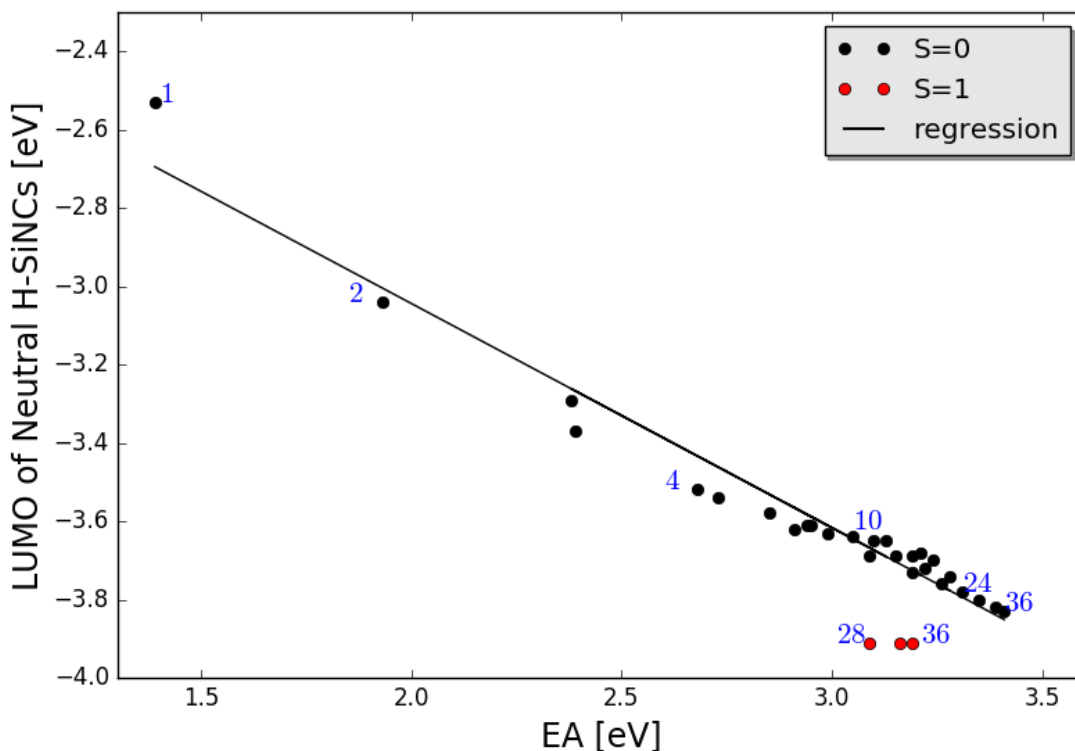


**Figure 6.** Correlation of the computed electron affinity (EA) for all H-SiNCs studied with the corresponding LUMO energy computed for the corresponding neutral H-SiNC. The numbers in the graph indicate the number of fused rings (N) for selected H-SiNCs. Here S represents the triplet and singlet states for  $S = 1$  and  $S = 0$ , respectively.

In Figure 6, the calculated LUMO energy level versus electron affinity for all H-SiNCs are shown. The data shows two different electronic configurations based on the initial ground states of the neutral molecules. First, we observe that there is a correlation between the electron affinity (EA) with the DFT-computed LUMO energies of the neutral species ( $E_{LUMO}$ ) with the corresponding initial spin state, having a linear regression of

$$E_{LUMO} = -0.573 * EA - 1.89 \text{ eV} \quad (5)$$

Where both  $E_{LUMO}$  and EA are in eV. The average absolute error in this relationship is 0.052 eV. The trend shows that LUMO energy levels generally decreased with increased EA. In addition, it

is noted that the EA increases as function of the number of fused rings ( $N$ ). These calculations indicate that both LUMO and EA can be independent to some extent, for instance, with respect to the number of fused rings.

## Summary and Outlook

In this study, we have shown that low hole and electron reorganization energies of H-SiNCs can be obtained. The most straightforward way of reducing these reorganization energies was achieved by increasing the number of fused rings,  $N$ . This is due to the extended  $\pi$  conjugation of H-SiNCs. It was further found that there exists an inverse dependence between the electron reorganization energy and the number of fused rings. Moreover, silicene nanoclusters are promising candidates as electron acceptors ( $n$ -type) because they have high electron affinities and low reorganization energies for electron transfer, which result from a large conjugated system. EA and  $\lambda$  can be further optimized by extending conjugation either through increasing the size of the system or by picking a specific direction, i.e., zigzag or armchair. We can also conclude that the spin state makes a significant change to the reorganization energy for corresponding silicene nanoclusters with  $n_1 > n_2$ . In addition, the percentage of nonbonding character could play a crucial role in the internal reorganization. Therefore, understanding the charge transport mechanism in terms of reorganization energies of these H-SiNCs is a key point for the design and stability of H-SiNCs electronic components.

Moreover, having explored the reduction of the reorganization energy through two methods, we suggest another strategy for reducing the reorganization energy: the application of constraints that prevents or minimizes the restructuring (distortions) along the vertical axes for the silicene nanoclusters. For instance, we could apply some constraints to the silicene nanocluster with the advantage of using atomically thin Van der Waals materials and their ability to form heterostructures. This exploits the fact that these heterostructures can form junctions that are

composed of *p*- and *n*-type semiconductors, each one being one unit cell thick, which exhibit completely different charge transport characteristics than bulk heterojunctions<sup>42</sup>. Thus, we can realize a *p-n* junction by using individually contacted layers of *p*-type tungsten diselenide<sup>43</sup> and the *n*-type silicene nanoclusters to create an atomically thin *p-n* junction. This type of heterostructure would need to encapsulate the silicene nanoclusters within a rigid matrix that could avoid structural rearrangements. The encapsulation with other 2D materials such as graphene and hBN layers could additionally avoid that these silicene nanoclusters became oxidized as it has been done for phosphorene<sup>44</sup>. Other effective ways to protect the silicene nanoclusters of oxidation are: (i) using a non-reactive in situ capping procedure that protect the silicene nanocluster by means of reactive molecular beam deposition of Al<sub>2</sub>O<sub>3</sub><sup>45</sup>; (ii) the silicene nanoclusters can be covered with polymers such as PMMA<sup>46</sup>, and (iii) depositing metal-ions on top of silicene nanoclusters which could increase the stability and transistor performance of the silicene nanoclusters<sup>47</sup>. Finally, these types of systems may lead to unique material platforms of novel, high-performance electronic and optoelectronic devices.

## AUTHOR INFORMATION

### Corresponding Author

\*To whom correspondence should be addressed. Email: [tvan@mit.edu](mailto:tvan@mit.edu)

### Author Contributions

All authors have given approval to the final version of the manuscript.

### Notes

The authors declare no competing financial interest.

¶ Deceased author.

## ACKNOWLEDGMENT

R.P.-P. would like to thank Millie Dresselhaus for several fruitful discussions over the weekends. R.P.-P. is also grateful to R. Olivares-Amaya for discussions on reorganization energy in organic systems. M.S.D., J. K., and R.P.-P. acknowledge the King Abdullah University of Science and Technology for support under contract (OSR- 2015-CRG4-2634). H.L.R. and S.F. acknowledge financial support from CONACyT (Grant 251684). J.L.M.C. acknowledges start-up funds from Florida State University and the Energy and Material Initiative and facilities at the High Performance Material Institute.

## APPENDIX A: DFT approximation

For the density functional approach, we use the B3LYP functional because it provided good results compared with experimental data. For instance, we compare bond-length alternation and torsional potentials using the results of disilane ( $\text{H}_3\text{Si-SiH}_3$ ). This B3LYP functional also gave encouraging results for the average calculated nearest Si-Si distance for a silicene nanoribbon on Ag(110) ( $2.24 \text{ \AA}$ )<sup>48</sup>. Furthermore, we compare the results of disilane ( $\text{H}_3\text{Si-SiH}_3$ ) using the B3LYP functional with others such as M062x and Perdew-Berke-Ernzerhof (PBE) functionals as shown in Table A1.

**Table A1.** Experimental and computed results for disilane. The cc-pVDZ basis set was used for all functionals.

Type	Experiment	<i>B3LYP</i>	<i>M062x</i>	PBE
$d_{\text{Si-Si}}[\text{\AA}]$	2.331 <sup>49</sup>	2.358	2.348	2.357
$d_{\text{Si-H}}[\text{\AA}]$	1.492 <sup>49</sup>	1.497	1.491	1.51
$\angle \text{Si-Si-H}$	110.3 <sup>50</sup>	110.3 <sup>°</sup>	110.2 <sup>°</sup>	110.3 <sup>°</sup>
$\angle \text{H-Si-H}$	108.6 <sup>50</sup>	108.7 <sup>°</sup>	108.8 <sup>°</sup>	108.6 <sup>°</sup>

Because of silicene's corrugated structure and due to B3LYP's inability to account for medium and long-range electron non covalent interactions we thought it necessary to implement DFT-D3 corrections to account for intramolecular London forces. Thereby, possibly gaining non-negligible corrections to our systems' overall energy. These corrections were ultimately negligible in comparison to the systems' kinetic and potential energies or otherwise were approximately the same for all cationic, anionic and neutral nanoclusters of the same  $n_z$  and  $n_a$  dimensions; canceling out whatever correction they might of had while obtaining their respective

relative energies, ionization potentials and electronic affinities. As a result of the lack of importance of vdW corrections, we can therefore assume that our results are not affected by the artificial stabilization brought on by the basis-set superposition error.

Moreover, in order to evaluate dispersion effects and torsion around the Si-Si bond, we substitute the hydrogen atoms in the disilane molecule with the mesityl group (Mes) to obtain the disilene molecule (Mes<sub>2</sub>Si=SiMes<sub>2</sub>). The results are shown in Table A2. As can be seen from Table A2, the B3LYP functional gives results which are in good agreement with the experimental results. Consequently, the B3LYP functional was chosen for geometrical optimizations of our silicene nanoclusters. This also shows that the torsional effect is not very significant for the cc-pVDZ basis which has no diffuse functions. Therefore, computations on anions without using diffuse functions could not change the results for our systems. **Additionally**, the introduction of diffuse functions markedly increases the computational cost of electronic structure methods and increases convergence difficulties.

**Table A2.** Experimental and computational results for Mes<sub>2</sub>Si=SiMes<sub>2</sub>. The cc-pVDZ basis set was used for all functionals.

Type	Experiment	B3LYP	M062x	PBE
$d_{Si-Si}[\text{Å}]$	2.16 <sup>51</sup>	2.16	2.14	2.19

In addition, to prove that our conclusions are not entirely dependent on the type of functional selected, we try to compare the results of B3LYP with different long-range corrected functionals. Then, we calculated the reorganization energies and adiabatic ionization potential as well as the adiabatic electronic affinity with different systems and different functionals to show that these values are not totally dependent on the functional used.

Usually long-range corrected (LRC) functionals are commonly used to enforce the computed molecular ionization potential (IP) to be equal to the negative energy of the HOMO of the neutral molecules ( $-E_{\text{HOMO}}$ ), i.e.  $r^1 = r^1(1-\text{erf}(\omega r)) + r^1\text{erf}(\omega r)$ . However, setting  $\omega$  to a fixed value is an approximation in itself, as  $\omega$  is a functional of the electron density<sup>52</sup>. Thereby, choosing the correct value of omega as well as a LRC functional is non trivial as  $\omega$  strongly depends on the system under study<sup>52,53</sup>. Moreover, the value of  $\omega$  that is optimal for ground state properties may not necessarily be optimal for excited state properties<sup>52,54</sup>. The criterion that LRC functionals should satisfy the known Koopman's theorem is given by<sup>55</sup>

$$-E_{\text{HOMO}}(\omega) = \text{IP}_v(\omega) \equiv E(N-1; \omega) - E(N; \omega) \quad (6)$$

where  $E_{\text{HOMO}}$  is the HOMO energy for a specific choice of  $\omega$  and IP is the ionization potential of an N electron system.

In Table A4, we have computed the delocalization error using Eq. 6 at the B3LYP/cc-pVDZ level of theory. As it can be seen, the delocalization error decreases with system size. Figure 7 illustrates the evolution of error in a series of selected nanoclusters from Table 2. As the silicene nanocluster grows from N=1 to N=32, the  $E_{\text{HOMO}}$  gradually approaches the calculated negative vertical ionization potential (IP<sub>v</sub>), leading to a smaller error bar than for the N=1.

**Table A4.** Vertical ionization potential (IP<sub>v</sub>) and the highest occupied molecular orbital energies ( $E_{\text{HOMO}}$ ) at the B3LYP/cc-pVDZ level for initial singlet states. Here,  $\text{DE} = E_{\text{HOMO}} + \text{IP}_v$ ; where DE is the delocalization error in eV.

H-SiNC( $n_z, n_d$ )	N	IP <sub>v</sub>	$E_{\text{HOMO}}$	DE
(1,1)	1	7.28	-5.71	1.57
(2,1)	2	6.57	-5.28	1.29
(3,1)	3	6.14	-5.04	1.09
(4,1)	4	5.86	-4.96	0.89
(5,1)	5	5.71	-4.94	0.77
(6,1)	6	5.64	-4.93	0.71
(7,1)	7	5.61	-4.93	0.68
(2,2)	4	6.14	-5.07	1.07
(3,2)	6	5.81	-4.88	0.93
(4,2)	8	5.61	-4.88	0.73

(5,2)	10	5.53	-4.88	0.65
(6,2)	12	5.52	-4.90	0.62
(7,2)	14	5.53	-4.91	0.62
(3,3)	9	5.61	-4.83	0.78
(4,3)	12	5.46	-4.82	0.64
(5,3)	15	5.45	-4.84	0.61
(6,3)	18	5.47	-4.88	0.59
(7,3)	21	5.42	-4.86	0.56
(4,4)	16	5.37	-4.79	0.58
(5,4)	20	5.39	-4.83	0.56
(6,4)	24	5.43	-4.84	0.59
(7,4)	28	5.33	-4.80	0.53
(4,5)	20	5.30	-4.76	0.54
(4,6)	24	5.26	-4.75	0.51
(4,7)	28	5.22	-4.73	0.49
(4,8)	32	5.18	-4.72	0.46
(4,9)	36	5.30	-4.71	0.59

---

To obtain an idea about the effect of long-range corrected (LC) functionals in our silicene nanoclusters, we use two typical values of  $\omega$  (in a.u.<sup>-1</sup>) which are  $\omega = 0.33$  as in refs. <sup>56,57</sup> and  $\omega = 0.5$  as in refs <sup>58,59</sup>. We consider two hybrids of PBE since PBE seems to benefit the most

from an admixture of HF exchange<sup>60</sup>. In addition, we use CAM-B3LYP functional which combines the hybrid qualities of B3LYP and the long-range correction presented by Tawada *et al.*<sup>56</sup>. The value of  $\omega$  was 0.33 which according to Tsuneda and co-workers gives improved results<sup>56,57</sup>.

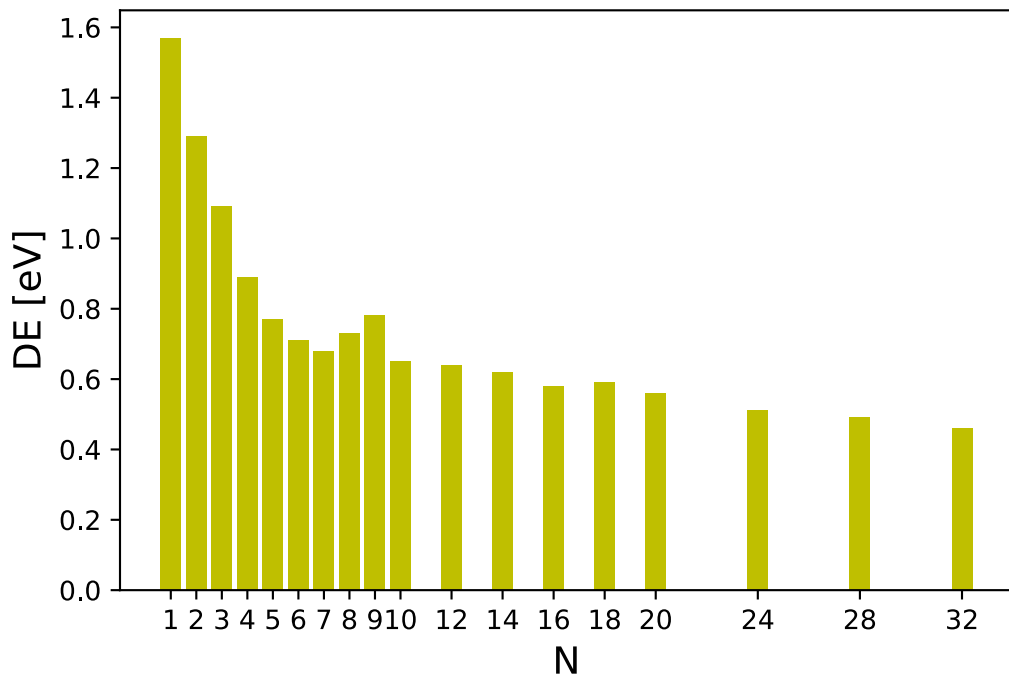


**Figure 7.** Deviations between the calculated  $E_{\text{HOMO}}$  and IP, for a series of selected H-SiNCs from table S4.

The numerical results were computed in Q-CHEM version 5.0<sup>61</sup> and Gaussian 16 electronic structure program. Turbomole (7.1) was not used for the long-range corrected functionals because its library does not contain them. We will indicate which calculations were performed in Q-CHEM, Gaussian and Turbomole with the following labels QChem5, Gaus16, and Turbo7, respectively.

We notice that there are a few changes in the values of reorganization energies using Turbomole (7.1) and Q-CHEM (5.0) at the same level of calculation (B3LYP/cc-pDVZ). This is because the implementation of the B3LYP exchange-correlation functional has the form of  $0.8 S + 0.72 B88 + 0.2 HF + 0.19 \underline{VWN(V)} + 0.81 LYP$  in Turbomole (7.1), which is the same functional form in the Gaussian program. In the case of Q-CHEM<sup>61</sup>, the B3LYP exchange-correlation functional has

the form of  $0.080 \text{ S} + 0.72 \text{ B88} + 0.2 \text{ HF} + 0.19 \text{ VWN1RPA} + 0.81 \text{ LYP}$ . Notice the difference for VWN(V) and VWN1RPA.

The comparison between values obtained from B3LYP with those obtained with PBE are shown Table A5. Both values are very similar. By comparing the B3LYP with LRC- $\omega$ PBE calculations at two different values of  $\omega$ , we observe that the LRC- $\omega$ PBE reorganization energies are higher than the ones obtained with B3LYP. However, the HOMO energies,  $E_{\text{HOMO}}$ , are larger than the IPs. This indicates that adding more long-range exact exchange than necessary, by optimally tuning for the Koopmans' theorem, will lead to a HOMO energy higher than the IP (sometimes called the localization error of HF), which is also observed in the localization error. In addition, we found that for LRC- $\omega$ PBE, tuning  $\omega$  in order to make  $\text{IP} = -E_{\text{HOMO}}$  leads to a  $\omega$  that decreases with increasing system size, meaning that less exact exchange could be used for larger molecules as done in other previous studies<sup>62,63</sup>. The latter can also be explained in terms of electron delocalization; electron delocalization increases along with molecule size, necessitating a smaller weight of exact exchange.

However, we note that when using CAM-B3LYP for H-SiNCs(5,1), we obtain a much higher hole reorganization energy than with LRC- $\omega$ PBE(QChem5) and B3LYP(QChem5). Noting that the delocalization error is smaller than 0.77 for the B3LYP/cc-vPDZ level. A possible caveat is that, we can not determine if this difference came from the implementation of B3LYP in Q-Chem. To remove this doubt, we test a larger nanocluster H-SiNCs(4,6) in Gaussian16. We used Gaussian16 in this part because B3LYP is implemented in the same way as in Turbomole 7.1. As we can see in this case, the hole reorganization energies are in the same value range with a delocalization error close to zero. In addition, spin contamination was a problem when we include the long-range corrected part. For instance, the spin contamination,  $S^2$ , of the radical cation of H-SiNCs(5,1) were 1.25 and 1.18 for CAM-B3LYP(QChem5) and LRC- $\omega$ PBE(QChem5), respectively. This problem was minor for the B3LYP functional with  $S^2=0.801$  which deviates only by 0.051 with the exact value  $S^2=0.750^31$ . The value of spin contamination for H-SiNCs(4,6) was  $S^2=3.37$  for CAM-B3LYP(Gaus16) indicating that wave function is mixing with a triplet state (see ref.<sup>31</sup>).

**Table A5.** Computed results for H-SiNC(1,1), H-SiNC(5,1) and H-SiNC(4,6). The cc-pVDZ basis set was used for all functionals. Here the delocalization errors are given as absolute value of  $\text{DE} = |E_{\text{HOMO}}(\omega) + \text{IP}_v(\omega)|$ . All results are given in eV.

Type	Functional	$\lambda_+$	$E_{\text{HOMO}}$	IP	IP <sub>v</sub>	DE
H-SiNCs(1,1)( <b>Turbo7</b> )	B3LYP	0.303	-5.71	7.12	7.28	1.57
H-SiNCs(1,1)( <b>QChem5</b> )	PBE	0.298	-5.34	7.24	7.39	2.06
H-SiNCs(1,1)( <b>QChem5</b> )	LRC- $\omega$ PBE	0.260	-7.95	7.23	7.38	0.57
	( $\omega = 0.5$ )					
H-SiNCs(1,1)( <b>QChem5</b> )	LRC- $\omega$ PBE	0.240	-7.66	7.24	7.36	0.30
	( $\omega = 0.3$ )					
H-SiNCs(1,1)( <b>QChem5</b> )	LRC- $\omega$ PBEh	0.245	-8.32	7.74	7.87	0.45
	( $\omega = 0.3$ )					
H-SiNCs(1,1)( <b>QChem5</b> )	CAM-B3LYP	0.256	-6.77	7.14	7.28	0.513
H-SiNCs(5,1)( <b>Turbo7</b> )	B3LYP	0.099	-4.94	5.66	5.71	0.77
H-SiNCs(5,1)( <b>QChem5</b> )	B3LYP	0.140	-4.88	5.70	5.76	0.88
H-SiNCs(5,1)( <b>Turbo7</b> )	PBE	0.096	-4.64	5.74	5.79	1.14
H-SiNCs(5,1)( <b>QChem5</b> )	PBE	0.099	-4.63	5.73	5.79	1.16
H-SiNCs(5,1)( <b>QChem5</b> )	LRC- $\omega$ PBE	0.179	-6.32	5.74	5.83	0.49
	( $\omega = 0.3$ )					
H-SiNCs(5,1)( <b>QChem5</b> )	CAM-B3LYP	0.220	-5.56	5.60	5.70	0.14
H-SiNCs(4,6)( <b>Turbo7</b> )	B3LYP	0.065	0.287	5.22	3.31	0.514
H-SiNCs(4,6)( <b>Gaus16</b> )	CAM-B3LYP	0.097	-5.865	5.87	5.92	0.05

While equation (7) has been shown to be useful for determining IPs, we can also adapt Koopmans's theorem for computing the electron affinity (EA) for IP of the N+1 electron system. In the case of using  $\omega$  that minimizes the overall derivation expressed in the target function, we use the following expression <sup>62</sup>:

$$J(\omega) = |E_{\text{HOMO}}(N, \omega) + \text{IP}(N, \omega)| + |E_{\text{HOMO}}(N+1, \omega) + \text{IP}(N+1, \omega)| \quad (8)$$

The down-side of using Eq. (8) is that the optimal value of  $\omega$  needs to be determined for each system of interest separately. The IP(N+1) can be related with the electron affinity (EA) of a N electron system.

Using Eq. 8, we compute J for EAs in the respective silicene nanoclusters presented in Table A6. According to Table A6, pure density functional approximations, B3LYP and PBE, predict more positive HOMO energies in anions than LRC functionals, which can be seen by observing the  $E_{\text{HOMO}}(\text{N}+1)$ . Adding a certain amount of HF exchange makes more negative all occupied orbital energies. However, the J error is larger than DEs, meaning that the EAs seems not to benefit at all from the admixture of the exact HF exchange, especially for the larger silicene nanocluster H-SiNCs(4,6) as shown in Table A6. When a finite basis set is used, the highest occupied orbital seems artificially stabilized irrespective of the value and sign of the orbital eigenvalue. This is the success of density functional approximations in predicting EAs which seems to rest on basis set effects and error cancellations, which do not necessarily comply to theoretical justifications for our case.

In conclusion, we demonstrate that the results obtained with B3LYP functional are not artifacts after comparing the results with some LRC functionals. The results shown in table A5 and A6 demonstrate that: the error in IPs can be only slightly reduced by using a long-corrected functional. For EAs, an admixture of HF exchange in any form increases the error.

**Table A6.** Computed results for H-SiNC(1,1), H-SiNC(5,1) and H-SiNC(4,6). The cc-pVDZ basis set was used for all functionals. All results are given in eV.

Type	Functional	$\lambda_-$	$E_{\text{HOMO}}(\text{N}+1)$	IP(N+1)	J	DE
H-SiNCs(1,1) ( <b>Turbo7</b> )	B3LYP	0.775	-0.253	1.39	2.71	1.57
H-SiNCs(1,1) ( <b>QChem5</b> )	PBE	0.853	-0.038	1.60	3.62	2.06
H-SiNCs(1,1) ( <b>QChem5</b> )	LRC- $\omega$ PBE	1.59	-2.99	1.80	1.77	0.57
	( $\omega = 0.5$ )					
H-SiNCs(1,1) ( <b>QChem5</b> )	LRC- $\omega$ PBEh	1.51	-3.08	1.95	1.58	0.45
	( $\omega = 0.3$ )					
H-SiNCs(5,1) ( <b>Turbo7</b> )	B3LYP	0.088	-2.10	2.85	1.52	0.77
H-SiNCs(5,1) ( <b>QChem5</b> )	B3LYP	0.129	-2.18	2.99	1.70	0.88
H-SiNCs(5,1) ( <b>Turbo7</b> )	PBE	0.091	-1.98	3.09	2.26	1.14

H-SiNCs(5,1)( <b>QChem5</b> )	PBE	0.093	-1.98	3.09	2.27	1.16
H-SiNCs(5,1)( <b>QChem5</b> )	LRC- $\omega$ PBE	0.296	-3.68	3.14	1.02	0.49
	( $\omega = 0.3$ )					
H-SiNCs(5,1)( <b>QChem5</b> )	CAM-B3LYP	0.440	-2.95	3.07	0.25	0.14
H-SiNCs(4,6)( <b>Turbo7</b> )	B3LYP	0.287	-2.82	3.31	1.00	0.514
H-SiNCs(4,6)( <b>Gaus16</b> )	CAM-B3LYP	0.496	-3.22	2.93	0.34	0.05

## References

1. Xia, F., Farmer, D. B., Lin, Y. M. & Avouris, P. Graphene field-effect transistors with high on/off current ratio and large transport band gap at room temperature. *Nano Lett.* **10**, 715–718 (2010).
2. Arco, L. G. De *et al.* Continuous , Highly Flexible , and Transparent Graphene Films by Chemical Vapor Deposition for Organic Photovoltaics. *ACS Nano* **4**, 2865–2873 (2010).
3. Varghese, S. S., Lonkar, S., Singh, K. K., Swaminathan, S. & Abdala, A. Recent advances in graphene based gas sensors. *Sensors Actuators, B Chem.* **218**, 160–183 (2015).
4. Raccichini, R., Varzi, A., Passerini, S. & Scrosati, B. The role of graphene for electrochemical energy storage. *Nat. Mater.* **14**, 271–9 (2015).
5. Qiao, J., Kong, X., Hu, Z.-X., Yang, F. & Ji, W. High-mobility transport anisotropy and linear dichroism in few-layer black phosphorus. *Nat. Commun.* **5**, 4475 (2014).
6. Radisavljevic, B. *et al.* Single-layer MoS<sub>2</sub> transistors. *Nat Nano* **6**, 147–150 (2011).
7. Cahangirov, S., Topsakal, M., Akturk, E., Sahin, H. & Ciraci, S. Two- and one-dimensional honeycomb structures of silicon and germanium. *Phys. Rev. Lett.* **102**, 236804 (2009).
8. Pablo-Pedro, R., Lopez-Rios, H., Fomine, S. & Dresselhaus, M. S. Detection of Multiconfigurational States of Hydrogen-Passivated Silicene Nanoclusters. *J. Phys. Chem. Lett.* **8**, 615–620 (2017).
9. Ding, Y. & Ni, J. Electronic structures of silicon nanoribbons. *Appl. Phys. Lett.* **95**, 83113–83115 (2009).
10. Tao, L. *et al.* Silicene field-effect transistors operating at room temperature. *Nat. Nanotechnol.* **10**, 227–231 (2015).
11. Wang, Y. *et al.* Half-metallic Silicene And Germanene Nanoribbons: Towards High-performance Spintronics Device. *Nano* **7**, 1250037-- (2012).
12. Wang, W. L., Meng, S. & Kaxiras, E. Graphene NanoFlakes with large spin. *Nano Lett.* **8**, 244–245 (2008).

13. Campos, L. C., Manfrinato, V. R., Sanchez-Yamagishi, J. D., Kong, J. & Jarillo-Herrero, P. Anisotropic etching and nanoribbon formation in single-layer graphene. *Nano Lett.* **9**, 2600–2604 (2009).
14. Schön, J. H., Kloc, C. & Batlogg, B. Universal crossover from band to hopping conduction in molecular organic semiconductors. *Phys. Rev. Lett.* **86**, 3843–3846 (2001).
15. Bredas, J. L., Calbert, J. P., da Silva Filho, D. A. & Cornil, J. Organic semiconductor: A theoretical characterization of the basic parameters governing charge transport. *Proc. Natl. Acad. Sci.* **99**, (2002).
16. Oboyle, N. M., Campbell, C. M. & Hutchison, G. R. Computational design and selection of optimal organic photovoltaic materials. *J. Phys. Chem. C* **115**, 16200–16210 (2011).
17. Hutchison, G. R., Ratner, M. A. & Marks, T. J. Intermolecular charge transfer between heterocyclic oligomers. Effects of heteroatom and molecular packing on hopping transport in organic semiconductors. *J. Am. Chem. Soc.* **127**, 16866–16881 (2005).
18. Devos, a & Lannoo, M. Electron-phonon coupling for aromatic molecular crystals: Possible consequences for their superconductivity. *Phys. Rev. B - Condens. Matter* **58**, 8236–8239 (1998).
19. Brédas, J.-L. J.-L. *et al.* Charge-Transfer and Energy-Transfer Processes in pi-Conjugated Oligomers and Polymers: A Molecular Picture. *Chem. Rev.* **104**, 4971–5003 (2004).
20. Sancho-García, J. C. & Pérez-Jiménez, a J. Charge-transport properties of prototype molecular materials for organic electronics based on graphene nanoribbons. *Phys. Chem. Chem. Phys.* **11**, 2741–6 (2009).
21. Larsson, S., Klimkans, A., Rodriguez-Monge, L. & Duskesas, G. Reorganization energies in organic pi systems. *Theochem-Journal Mol. Struct.* **425**, 155–159 (1998).
22. Sun, Y.-P., Wang, P. & Hamilton, N. B. Fluorescence Spectra and Quantum Yields of Buckminsterfullerene (C60) in Room-Temperature Solutions. No Excitation Wavelength Dependence? *J. Am. Chem. SOC* **115**, 6378–6381 (1993).
23. Coropceanu, V. *et al.* Hole- and electron-vibrational couplings in oligoacene crystals: intramolecular contributions. *Phys. Rev. Lett.* **89**, 275503 (2002).
24. Xu, M., Liang, T., Shi, M. & Chen, H. Graphene-Like Two-Dimensional Materials. *Chem. Rev.* **113**, 3766–3798 (2013).
25. Wang, Q. H., Kalantar-Zadeh, K., Kis, A., Coleman, J. N. & Strano, M. S. Electronics and optoelectronics of two-dimensional transition metal dichalcogenides. *Nat. Nanotechnol.* **7**, 699–712 (2012).
26. Ling, X., Wang, H., Huang, S., Xia, F. & Dresselhaus, M. S. The renaissance of black phosphorus. *Proc. Natl. Acad. Sci.* **112**, 4523–4530 (2015).
27. Rudenko, A. N., Brener, S. & Katsnelson, M. I. Intrinsic Charge Carrier Mobility in Single-Layer Black Phosphorus. *Phys. Rev. Lett.* **116**, 246401 (2016).
28. Grimme, S., Antony, J., Ehrlich, S. & Krieg, H. A consistent and accurate ab initio parametrization of density functional dispersion correction (DFT-D) for the 94 elements H-Pu. *J. Chem. Phys.* **132**, 154104 (2010).

29. Noodleman, L. Valence bond description of antiferromagnetic coupling in transition metal dimers. *J. Chem. Phys.* **74**, 5737 (1981).
30. TURBOMOLE V7.0 2015, a development of University of Karlsruhe and Forschungszentrum Karlsruhe GmbH, 1989-2007, TURBOMOLE GmbH, since 2007; available from <http://www.turbomole.com>.
31. See Supplemental Material at ... for CASSCF calculations for the system that present an initial triplet state. In addition, a detailed discussion of the spin contamination for the cations and anions is given.
32. Frisch, M. J.; Trucks, G. W.; Schlegel, H. B.; Scuseria, G. E.; Robb, M. A.; Cheeseman, J. R.; Scalmani, G.; Barone, V.; Mennucci, B.; Petersson, G. A.; Nakatsuji, H.; Caricato, M.; Li, X.; Hratchian, H. P.; Izmaylov, A. F.; Bloino, J.; Zheng, G.; Sonnenb, D. J. Gaussian 09, revision D.01; Gaussian Inc.: Wallingford, CT. (2013).
33. Chang, Y. C. & Chao, I. An important key to design molecules with small internal reorganization energy: Strong nonbonding character in frontier orbitals. *J. Phys. Chem. Lett.* **1**, 116–121 (2010).
34. Gruhn, N. E. *et al.* The vibrational reorganization energy in pentacene: Molecular influences on charge transport. *J. Am. Chem. Soc.* **124**, 7918–7919 (2002).
35. Amashukeli, X., Winkler, J. R., Gray, H. B., Gruhn, N. E. & Lichtenberger, D. L. Electron-transfer reorganization energies of isolated organic molecules. *J. Phys. Chem. A* **106**, 7593–7598 (2002).
36. Jonathan C. Rienstra-Kiracofe and Henry F. Schaefer, G. S. T. Atomic and Molecular Electron Affinities: Photoelectron Experiments and Theoretical Computations. *Chem. Rev.* **102**, 231–282 (2002).
37. Kuo, M. Y., Chen, H. Y. & Chao, I. Cyanation: Providing a three-in-one advantage for the design of n-type organic field-effect transistors. *Chem. - A Eur. J.* **13**, 4750–4758 (2007).
38. Chang, Y.-C., Kuo, M.-Y., Chen, C.-P., Lu, H.-F. & Chao, I. On the Air Stability of n-Channel Organic Field-Effect Transistors: A Theoretical Study of Adiabatic Electron Affinities of Organic Semiconductors. *J. Phys. Chem. C* **114**, 11595–11601 (2010).
39. Newman, C. R., Frisbie, C. D., Demetrio, A., Filho, S. & Bre, J. Introduction to Organic Thin Film Transistors and Design of n-Channel Organic Semiconductors. *Chem. Mater.* **16**, 4436–4451 (2004).
40. Facchetti, A., Yoon, M. H., Stern, C. L., Katz, H. E. & Marks, T. J. Building blocks for n-type organic electronics: Regiochemically modulated inversion of majority carrier sign in perfluoroarene-modified polythiophene semiconductors. *Angew. Chemie - Int. Ed.* **42**, 3900–3903 (2003).
41. Zade, S. S. & Bendikov, M. Study of hopping transport in long oligothiophenes and oligoselenophenes: Dependence of reorganization energy on chain length. *Chem. - A Eur. J.* **14**, 6734–6741 (2008).
42. Lee, C.-H. *et al.* Atomically thin p–n junctions with van der Waals heterointerfaces. *Nat. Nanotechnol.* **9**, 676–681 (2014).
43. Yu, X., Prévot, M. S., Guijarro, N. & Sivula, K. Self-assembled 2D WSe<sub>2</sub> thin films for photoelectrochemical hydrogen production. *Nat. Commun.* **6**, 7596 (2015).

44. Li, L. *et al.* Direct observation of the layer-dependent electronic structure in phosphorene. *Nat. Nanotechnol.* **12**, 21–25 (2017).
45. Molle, A. *et al.* Hindering the oxidation of silicene with non-reactive encapsulation. *Adv. Funct. Mater.* **23**, 4340–4344 (2013).
46. Koenig, S. P. *et al.* Electric field effect in ultrathin black phosphorus Electric field effect in ultrathin black phosphorus. **103106**, (2015).
47. Guo, Z. *et al.* Metal-Ion-Modified Black Phosphorus with Enhanced Stability and Transistor Performance. *Adv. Mater.* **29**, 1–8 (2017).
48. Aufray, B. *et al.* Graphene-like silicon nanoribbons on Ag(110): A possible formation of silicene. *Appl. Phys. Lett.* **96**, 1–4 (2010).
49. Eliel, E. L. *Stereochemistry of Organic Compounds.* (Wiley).
50. Dahlqvist, K. I. & Forsén, S. The barrier to internal rotation in 2-furanaldehyde. *J. Phys. Chem.* **69**, 4062–4071 (1965).
51. Raabe, G. & Michl, J. Multiple Bonding to Silicon. *Chem. Rev.* **85**, 419–509 (1985).
52. Baer, R., Livshits, E. & Salzner, U. Tuned Range-Separated Hybrids in Density Functional Theory. *Annu. Rev. Phys. Chem.* **61**, 85–109 (2010).
53. Baer, R. & Neuhauser, D. Density functional theory with correct long-range asymptotic behavior. *Phys. Rev. Lett.* **94**, 2–5 (2005).
54. Rohrdanz, M. A., Martins, K. M. & Herbert, J. M. A long-range-corrected density functional that performs well for both ground-state properties and time-dependent density functional theory excitation energies, including charge-transfer excited states. *J. Chem. Phys.* **130**, (2009).
55. Kuritz, N., Stein, T., Baer, R. & Kronik, L. Charge-transfer-like  $\pi \rightarrow \pi^*$  excitations in time-dependent density functional theory: A conundrum and its solution. *J. Chem. Theory Comput.* **7**, 2408–2415 (2011).
56. Tawada, Y., Tsuneda, T., Yanagisawa, S., Yanai, T. & Hirao, K. A long-range-corrected time-dependent density functional theory. *J. Chem. Phys.* **120**, 8425–8433 (2004).
57. Kamiya, M., Tsuneda, T. & Hirao, K. A density functional study of van der Waals interactions. *J. Chem. Phys.* **117**, 6010–6015 (2002).
58. Gerber, I. C. & Ángyán, J. G. Hybrid functional with separated range. *Chem. Phys. Lett.* **415**, 100–105 (2005).
59. Lngyaln, J. G., Gerber, I. C., Savin, A. & Toulouse, J. Van der Waals forces in density functional theory: Perturbational long-range electron-interaction corrections. *Phys. Rev. A - At. Mol. Opt. Phys.* **72**, 1–9 (2005).
60. Ernzerhof, M. & Scuseria, G. E. Assessment of the Perdew–Burke–Ernzerhof exchange–correlation functional. *J. Chem. Phys.* **110**, 5029–5036 (1999).
61. Shao, Y. *et al.* Advances in molecular quantum chemistry contained in the Q-Chem 4 program package. *Mol. Phys.* **113**, 184–215 (2015).

62. Stein, T., Eisenberg, H., Kronik, L. & Baer, R. Fundamental gaps in finite systems from eigenvalues of a generalized Kohn-Sham method. *Phys. Rev. Lett.* **105**, 1–4 (2010).
63. Salzner, U. & Aydin, A. Improved prediction of properties of  $\pi$ -conjugated oligomers with range-separated hybrid density functionals. *J. Chem. Theory Comput.* **7**, 2568–2583 (2011).